Earth and Planetary Science Letters 317-318 (2012) 1–7

Contents lists available at SciVerse ScienceDirect

Earth and Planetary Science Letters

journal homepage: www.elsevier.com/locate/epsl

Simulating rotating fluid bodies: When is vorticity generation via density-stratification important?

M. Evonuk *, H. Samuel

Bayerisches Geoinstitut, Universität Bayreuth, D-95440 Bayreuth, Germany

ARTICLE INFO

Article history:
Received 1 September 2011
Received in revised form 9 November 2011
Accepted 24 November 2011
Available online 26 December 2011

Editor: T. Spohn

Keywords:
numerical modeling
convection
density stratification
hydrodynamics
differential flow
Earth's core

ABSTRACT

Differential rotation is one of the key components needed to maintain a magnetic dynamo, therefore it is important to understand the processes that generate differential rotation in rotating bodies. In a rotating density-stratified fluid, local vorticity generation occurs as fluid parcels move radially, expanding or contracting with respect to the background density stratification. The convergence of this vorticity forms zonal flow structures as a function of the radius and the slope of the background density profile. While this effect is thought to be of importance in bodies that are quickly rotating and highly turbulent with large density stratifications such as Jupiter, it is generally neglected in bodies such as the Earth's outer core, where the density change is small. Simulations of thermal convection in the 2D rotating equatorial plane are conducted to determine the parameter regime where local vorticity generation plays a significant role in organizing the fluid flow. Three regimes are found: a dipolar flow regime, where the flow is not organized by the rotation, a transitional flow regime, and a differential flow regime, where the flow is strongly organized into differential rotation with multiple jets. A scaling law is determined based on the convective Rossby number and the density contrast across the equatorial plane, providing a simple way to determine in which regime a given body lies. While a giant planet such as Jupiter lies firmly in the differential flow regime as expected, the Earth's outer core is also found to lie in the differential flow regime indicating that, even in the Earth's outer core, where the density contrast is small, vorticity contributions via fluid movement through the density stratificationmay be non-negligible.

1. Introduction

Magnetic field generation and maintenance in planetary cores is an area of active research (Anufriev and Cupal, 2001; Aubert and Wicht, 2004; Glatzmaier and Roberts, 1996; Guervilly et al.; Olson and Christensen, 2006; Olson et al., 2010; Sarson and Jones, 1999; Schaeffer and Cardin, 2006; Stanley and Glatzmaier, 2010; Stanley et al., 2005). There are several ingredients that are thought to be key to maintaining a magnetic dynamo, rotation, a highly turbulent, three-dimensional helical flow, an electrically conducting fluid, and differential rotation. Dipole dominated magnetic fields, such as those seen on the Earth and Jupiter, occur in rotationally dominated fluid flows with strong differential rotation, whereas more inertial flows produce weaker fields with higher multi-pole components (Christensen and Aubert, 2006; Sreenivasan and Jones, 2006).

Deep shell differential rotation in rotating fluids has been simulated in 3D (Aurnou and Olson, 2001; Christensen, 2001, 2002; Glatzmaier, 2005; Heimpel et al., 2005; Jones and Kuzanyan, 2009; Kaspi et al., 2009), in the 2D meridional plane (Jones et al., 2003; Rotvig and Jones, 2006), and in the 2D equatorial plane (Evonuk, 2008). Mechanisms that can lead to differential flow in a rotating body are vortex stretching via Busse rolls and conservation of potential vorticity, or local generation of vorticity as fluid parcels move through a density stratification, hereafter referred to as the LVDS mechanism. Vortex stretching is a global mechanism which occurs regardless of density change, while LVDS is a local mechanism that occurs only in density-stratified fluids. Arguments have been presented indicating that a global mechanism is likely to become harder to maintain as a fluid becomes more turbulent (Glatzmaier et al., 2009) therefore favoring LVDS vorticity generation in extreme parameter regimes. Recent simulations in 3D compare the fluid behavior and heat flux in anelastic and Boussinesq models and find that anelastic simulations have significant baroclinic shear, disrupting the pure Taylor columns seen in Boussinesq simulations and that additional high latitude jets can form in the anelastic cases (Jones and Kuzanyan, 2009; Kaspi et al., 2009). This paper seeks to focus only on the effect of changing density as opposed to looking at both density and geometry simultaneously. Two-dimensional simulations in the equatorial plane, without additional terms to add the effect of curvature of the boundaries in the northern and southern hemispheres, eliminate any contribution to the vorticity from Busse rolls. Therefore, any zonal jet structures formed will result

* Corresponding author.
E-mail address: martha.evonuk@uni-bayreuth.de (M. Evonuk).
URL: http://www.staff.uni-bayreuth.de/~btgi96/Site/Home.html (M. Evonuk).

0012-821X/$ – see front matter © 2011 Elsevier B.V. All rights reserved.
doi:10.1016/j.epsl.2011.11.036

from vorticity generated by local interaction of the rotation with the density stratification, LVDS. For a detailed discussion on how these two mechanisms work see: Busse (1976), Glatzmaier and Evonuk (2006), Glatzmaier et al. (2009) and Evonuk (2008).

Previous simulations in the 2D equatorial plane explored the relationship between Rayleigh number and Ekman number for a fluid with a large density stratification (density at the center of the simulations 56 times greater than the density at outer edge) (Evonuk, 2008). Evonuk (2008) found that decreasing the driving (decreasing Rayleigh number) and/or increasing the rotation rate (decreasing Ekman number) from a mid-case with two jets led to a larger numbers of jets with radius, that is, further into a differential flow regime, while the opposite (increasing Rayleigh and Ekman numbers) led to a dipolar flow regime, where the fluid did not feel the effect of rotation and the dominant fluid flow was directly through the center of the equatorial plane forming two cells. While Evonuk (2008) demonstrated that LVDS vorticity generation was likely important for Jovian planets, which have large density contrasts, this study did not establish how the strength of the LVDS effect depends on the total contrast in the background density profile.

In order to make the results of Evonuk (2008) more general, and scalable to other density contrasts and therefore to arbitrary bodies, this study is expanded to explore in addition to the effects of Rayleigh number and Ekman number, the effects of the density contrast and the Prandtl number. A quantity C is then calculated from the Ekman number, Rayleigh number, Prandtl number and density contrast, which is seen to correlate to the flow regime of the fluid. High values of titC are indicative of dipolar flow (rotation and/or density stratification not important) while low C values correspond to differential flow (rotationally dominated, where LVDS vorticity generation is important). The predicted value of xtitC for the Earth's liquid core, in spite of its small change of density, lies in the regime of differential flow, indicating LVDS may play an important role in generating differential rotation in the Earth's outer core, and therefore in generating and maintaining the Earth's geomagnetic field.

Again, simulations are restricted to two dimensions, not only to explore parameter regimes difficult or impossible to reach in 3D, but to focus on the LVDS mechanism and to allow a systematic exploration of the parameter space.

2. Numerics

The thermal-convection simulations are performed using a modified version of the Evonuk–Glatzmaier finite-volume code on a Cartesian grid in 2D (Evonuk and Glatzmaier, 2006). The basic anelastic equations solved are non-dimensional versions of the momentum (1), conservation of mass (2), and energy (3) equations:

$$\frac{\partial}{\partial t}(\bar{\rho}\mathbf{u}) = -\nabla\cdot\left[\bar{\rho}u_i u_j + p\delta_{ij} - 2Pr\bar{\rho}\left(e_{ij} - \frac{1}{3}(\nabla\cdot\mathbf{u})\delta_{ij}\right)\right] + \left(\frac{RaPr}{K}\frac{d\bar{\rho}}{dr}\bar{T}S + \frac{d\bar{\rho}}{dr}\frac{1}{\bar{\rho}}p\right)\hat{r} + \frac{Pr}{Ek}\bar{\rho}\mathbf{u}\times\Omega, \tag{1}$$

$$\nabla\cdot(\bar{\rho}\mathbf{u}) = 0, \tag{2}$$

$$\frac{\partial}{\partial t}(\bar{\rho}S) = -\nabla\cdot(\bar{\rho}\mathbf{u}S - \bar{\rho}\nabla S) + \frac{\bar{\rho}}{\bar{T}}\frac{d\bar{T}}{dr}\left(\frac{\partial S}{\partial r}\right) + \bar{\rho}Q_s, \tag{3}$$

where t is the non-dimensional time, $\bar{\rho}$ is the background density profile, $\mathbf{u}$ is the velocity vector, p is the pressure, δ_{ij} is the Kronecker delta, e_{ij} is the viscous stress tensor, $\hat{r}$ is the unit vector in the radial direction, Ω is a unit vector in the direction of the rotation axis (perpendicular to the equatorial plane), S is the entropy perturbation, $\bar{T}$ is the background temperature profile, and Q_s is the heating function. The energy Eq. (3) is written here in the form of an entropy equation using entropy diffusion. The units of length, time, pressure, temperature and entropy used to express the above equations in their non-dimensional form are D, D^2/κ, $\kappa^2\rho_o/D^2$, $1/\alpha$ and ΔS, where D is the radius of the disk, κ is the thermal diffusivity, ρ_o is the density at the center of the equatorial plane, α is the thermal expansion coefficient, and ΔS is the change in entropy across the disk.

The equations are characterized by several dimensionless numbers. The Rayleigh number,

$$Ra = \frac{g_o \Delta S D^3}{C_p \nu\kappa}, \tag{4}$$

is the ratio of the buoyancy terms to the diffusive terms, with g_o being the gravity at the outer edge of the equatorial plane, C_p the specific heat capacity, and ν the kinematic viscous diffusion. As the simulations do not include an inner core, and the total change in entropy, ΔS, is calculated from the output of the simulation. Higher Rayleigh numbers generally indicate higher driving and therefore more turbulent flows. The Rayleigh number is varied between several thousand to close to 10^9 and is calculated with a time averaged ΔS after the simulation has reached a statistical steady state. The Ekman number,

$$Ek = \frac{\nu}{2\Omega D^2}, \tag{5}$$

compares the viscous terms to the Coriolis term, here Ω is the rotation rate. Smaller Ekman numbers correspond to higher rotation rates or cases where the rotation more dominantly determines fluid behavior. The Ekman number is varied between 10^{-3} and 10^{-6}. The Prandtl number,

$$Pr = \frac{\nu}{\kappa}, \tag{6}$$

is the a ratio of the viscous to the thermal diffusivity. In all of the simulations the diffusivities were prescribed to be constant with radius. The Prandtl number is varied between 0.01 and 10 for a select number of cases, while the majority are runwith $Pr = 1.0$. The compressibility number of the fluid is

$$K = \frac{g_o \alpha D}{C_p \gamma}, \tag{7}$$

where γ is the Grüneisen parameter. Simulations are run with $K = 0.2$ and $\gamma = 0.5$, a value of the Grüneisen parameter appropriate for Saturn. The appropriate value of the compressibility for the Earth is also $K = 0.2$ (Anufriev et al., 2005), but with $\gamma = 1.5$ (Vočadlo et al., 2003). The Grüneisen parameter, γ, is also used to determine the background temperature profile, $\bar{T} = \bar{\rho}^{\ \gamma}$.

The background gravity, is based on the integration of the background density profile, $\bar{g}(r) = \frac{4\pi G}{r}\int_0^r \bar{\rho}(r) r dr$, where G is the gravitational constant and $\bar{\rho}$ is of the form $\bar{\rho} = \rho_o - C_1 r^2 + C_2 r^4$ with constants C_1 and C_2 determined by specifying the slope of the density profile at the origin and the outer boundary, both here taken to be zero. The density profile retains the shape used for the cases with larger density contrast and no core in Evonuk (2008), with density changing slowly near the center of the equatorial plane and more quickly near the outer edge. The density contrast in the background profile is quantified by $\chi_\rho = \rho_o/\rho_t$, where and ρ_t is the density at the outer edge of the equatorial plane. The density contrast, χ_ρ, is varied from 1.22 (appropriate for the Earth's outer core) to 7.39.

Simulations are viewed from the north, with eastward, prograde flow in the counterclockwise direction. All models are performed with a regular Cartesian grid resolution of 400×400 points. Boundary conditions are free-slip (via large source terms in the momentum solver) with the entropy perturbation set to zero on the outer edge of the equatorial plane. The heating function represents heat sources such as residual heat of formation or radioactive heating and in these

simulations spans the inner 35% of the disk and takes the form of a cosine function with peak values occurring at the origin and tapering to zero by 35% of the radius. An alternate constant heating function with radius, across the entire disk (not just in the inner 35%), is used for five cases with $\chi_\rho = 1.22$ to better approximate the heating distribution for the Earth's core and to determine if the heating function plays a role in the fluid flow patterns seen. Peak values of Q_s are 300 in both cases. All simulations are run without inner cores allowing fluid flow directly through the origin of the equatorial plane. Simulations are continued until their kinetic energies have reached a statistical steady state.

3. Results

Three basic regimes are noted for the simulation results. At one extreme is dipolar flow, where the fluid flows directly through the center of the equatorial plane, seemingly little influenced by the rotation (Fig. 1a, b). For comparison, Fig. 2 shows the tangential flow for two Boussinesq cases, where $\chi = 1.0$ and therefore rotation is unable to play a role in the 2D simulation. One can see, even at higher Rayleigh number where the flow becomes more turbulent, the bulk flow is still dipolar in nature. The dipolar flows tended to have ratios of azimuthal to radial kinetic energies on the order of one, though there were cases with ratios as high as three or four. At the other extreme is differential flow, where the fluid is strongly influenced by rotation and organizes into differential rotation with two or more jets forming a zonal flow structure with radius (Fig. 1e, f). The cases with differential flows tended to have ratios of tangential to radial kinetic energy on the order of tens, though some cases had ratios as small as five. An intermediary, transitional flow is also seen, where the fluid is influenced by the rotation but not strongly enough to form steady jets. In this regime the fluid often oscillates between dipolar flow structures and single jets centered on the origin ringed by smaller vortices or even quasi-two jet structures, where the outer jet does not fully encircle the inner jet (examples in Fig. 1c, d). The transitional flows were highly time dependent thus distinguishing themselves from the dipolar and differential flows. Likewise, also time dependent, were their ratios of tangential and radial kinetic energies ranging from values close to one to values in excess of several tens. Example (d) in Fig. 1 shows an extreme transitional case where the fluid is almost organized into a two-jet structure, while example (c) shows a more typical case with a jet at the origin, sometimes appearing dipolar and sometimes flanked by multiple smaller vortices. As expected from the results of Evonuk (2008) the basic trend of smaller Rayleigh numbers and smaller Ekman numbers corresponding to more rotationally dominated flow is seen for all values of the density contrast, χ_ρ. As an example, the results for $\chi_\rho = 3.00$ are plotted as a function of Rayleigh number versus Ekman number in Fig. 3. The transition between the regimes is well fit by a curve of $Ek \propto Ra^{-1/2}$ for all χ_ρ (shown in the dashed lines in Fig. 3).

Additional cases run at $\chi_\rho = 1.22$ with uniform heating show no significant change in behavior with cases falling in flow regimes as expected for their Ekman and Rayleigh numbers. An expanded graph, Fig. 4, shows the Earth-like density contrast, $\chi_\rho = 1.22$, including the results of uniform heating (open symbols) and the approximate locations of several terrestrial bodies (large open circles). Estimates for the Rayleigh number and Ekman number are based on the values of the convective depth and buoyancy fluxes from Olson and Christensen (2006) and on the assumption that the viscous and thermal diffusivities are similar in these bodies, which is likely not the case, especially not for Ganymede. While this density contrast is appropriate, or nearly so for Venus, Mars and the Earth, smaller values of χ_ρ in Mercury, the Moon, and Ganymede would result in a

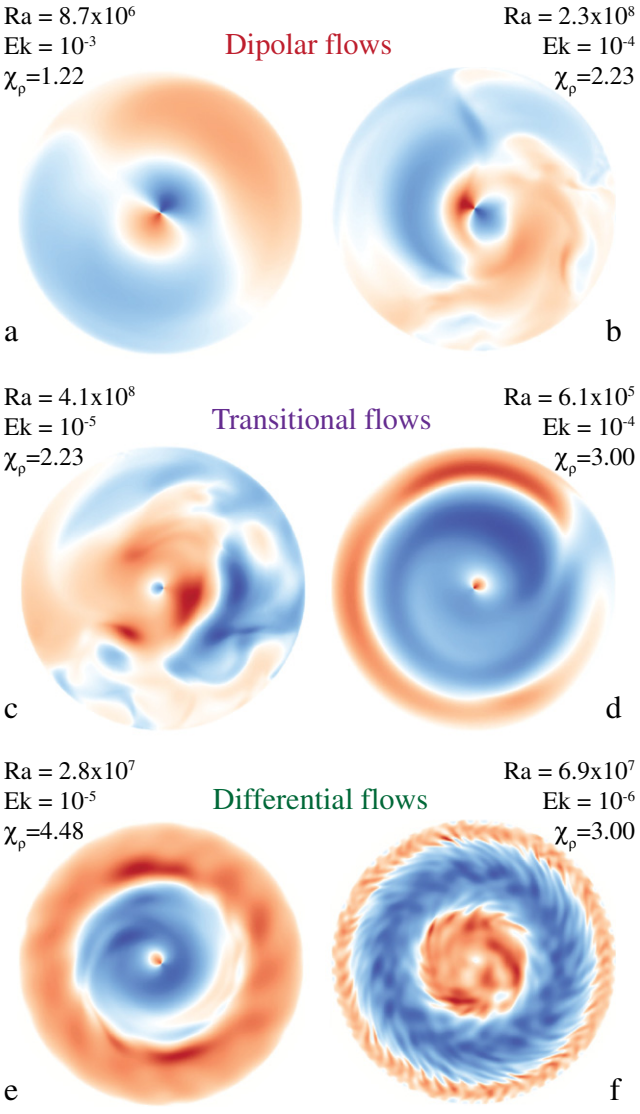

Fig. 1. Snap shots of the tangential fluid flow for six cases, red indicates prograde fluid flow (in the direction of rotation) and blue indicates retrograde fluid flow. Cases a and b demonstrate the flow pattern for two dipolar cases. Case a shows a very clear dipole, while case b shows additional small scale behavior near the outer rim of the disk due to the increase in the density contrast and the Rayleigh number. Cases c and d are transitional flows, case c being a more typical transitional flow with a central jet oscillating about the origin, while case d shows a transitional case which is almost a two jet structure. Cases e and f are in the differential flow regime with two and three jet zonal flows.

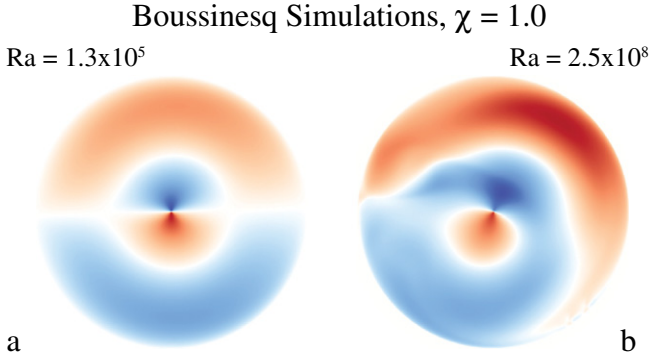

Fig. 2. Snap shots of the tangential fluid flow for two Boussinesq cases where $\chi = 1.0$, red indicates prograde fluid flow (in the direction of rotation) and blue indicates retrograde fluid flow as in Fig. 1. Both cases, low and high Rayleigh number, show a bulk flow that is clearly dipolar with flow directly through the origin forming two large cells. This is the pattern seen also in cases a and b of Fig. 1.

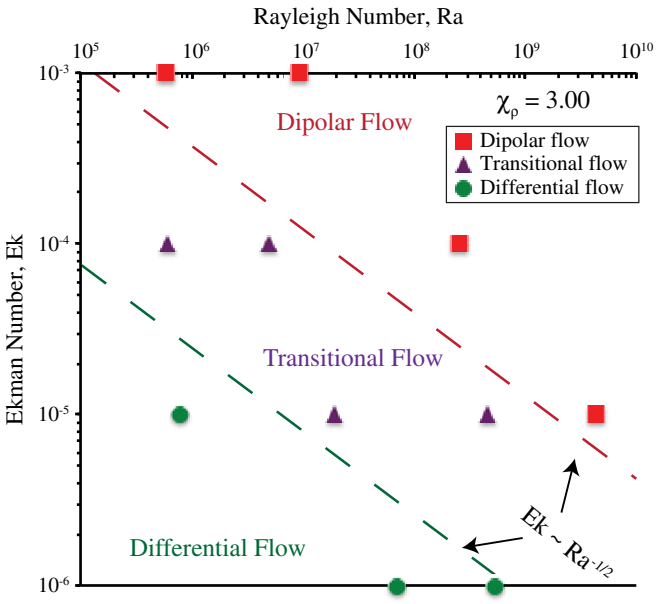

Fig. 3. Log–log plot of the Rayleigh number versus the Ekman number for a density contrast of 3.00 with $Pr = 1.0$. Red squares show cases with dipolar flow, purple triangles transitional flow, and green circles differential flow. Dashed lines indicate the transition between the three regions with the relationship $Ek \propto Ra^{-1/2}$.

relative shift to the right for these bodies with respect to the transition to differential flow. That is, larger χ_ρ transitions to differential flow at larger Ra and larger Ek than smaller χ_ρ. To quantify this, the results of cases at different χ_ρ need to be seen on one graph.

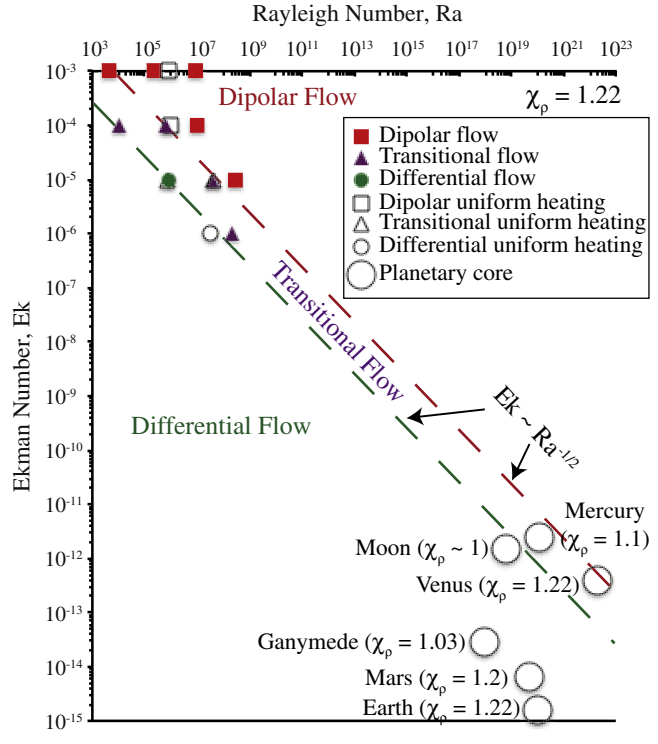

Fig. 4. Log–log plot of the Rayleigh number versus the Ekman number for a density contrast of 1.22 with $Pr = 1.0$ expanded to include the parameter regime of the terrestrial planets. Symbols are as defined in Fig. 3 with small open symbols indicating cases with uniform heating and large circular labeled symbols representing the planets. Dashed lines again mark the transition between the flow regimes with the relationship $Ek \propto Ra^{-1/2}$. We see that the planets are far from the regime modeled, however the trends indicate that most planets lie in the differential to transitional regimes.

In order to compare the results of all the simulations with their varying density contrasts and Prandtl numbers, the Rayleigh number, Ekman number, and Prandtl number are combined into a convective Rossby number, $Ro_c = Ek\sqrt{Ra/Pr}$ (Gilman, 1977). Generally it is assumed that a convective Rossby number less than one is where the effects of rotation become important, since in the time a fluid element is driven across a layer by buoyancy it can execute more than one inertial rotation (Brummell et al., 1998). This appears to be the case in 3D Boussinesq simulations in a free-slip box (Julien et al., 2001) and in 3D turbulent compressible simulations in a local f-plane model (Brummell et al., 1998), though the scaling changes in Boussinesq simulations with no-slip boundary conditions as the boundary layers become important (Stellmach and Hansen, 2010). Others have found it may be that the crossover occurs nearer the value of two (Schmitz and Tilgner, 2009), or in the case of boundary-layer-controlled transition scaling it occurs at values less than Ro_c (King et al., 2009). Regardless of the exact cutoff, smaller values of convective Rossby number indicate a greater influence of rotation on the fluid dynamics while larger values indicate that buoyancy is dominant. The transition from dipolar flow to differential flow occurs at convective Rossby numbers much smaller than one for most of the simulations shown here ($\chi_\rho = 1.22 - 7.39$), though the boundary between dipolar and transitional cases for $\chi_\rho = 7.39$ does occur close to $Ro_c = 1$, which can be seen in Fig. 5.

The results plotted as the density contrast versus the convective Rossby number show a clear trend between dipolar flow, transitional flow and differential flow (Fig. 5), dashed lines here (and in Fig. 7) have a best fit for $Ro_c \propto \chi_\rho^{3/2}$. It is noted that higher Prandtl numbers act to push the flow towards more rotationally dominated behavior. This is expected as higher Prandtl numbers correspond to weakening inertia. Cases with Prandtl number not equal to one, as well as the corresponding case with $Pr = 1.0$, are noted in Fig. 5. As the fluid behavior in these cases with $Pr \neq 1$ continue to follow the previous pattern with convective Rossby number, it seems likely that Ro_c and χ_ρ are good criteria for noting this transition between flow patterns.

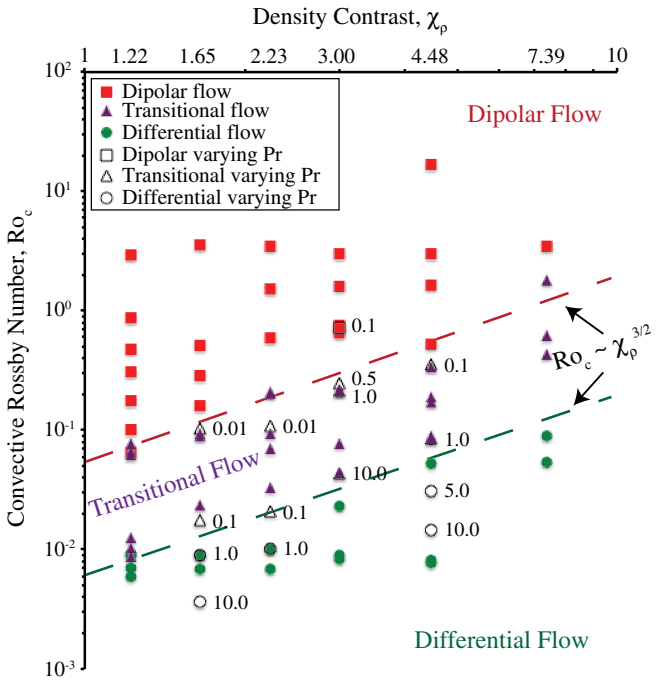

Fig. 5. Log–log plot of density contrast versus convective Rossby number. Symbols are as defined in Fig. 3 with filled symbols indicating cases with $Pr = 1.0$ and open symbols indicating cases where the Prandtl number is varied (the equivalent cases with $Pr = 1.0$ are shown as filled symbols lined in black). Uniform heating cases for $\chi_\rho = 1.22$ are included but not highlighted. Dashed lines demarcate the transition between the flow regimes with the relationship $Ro_c \propto \chi_\rho^{3/2}$.

As the Rayleigh number increases, so do the mean velocities, as higher Rayleigh numbers correspond to larger driving forces. The majority of the simulations in this study had only two jets and on average the mean zonal velocities for the cases with only two jets appear to scale as approximately $Ra^{2/3}\chi^2$, shown in (Fig. 6), where the exponents are a best fit to the simulation results. There is one obvious outlier, the case with uniform heating which implies that the heating distribution is a contributing factor in the strength the mean zonal flow. This trend merits further study as the number of data points is small. This is especially true for the cases with larger numbers of jets of which there are only two representative cases, which prevents any scaling for the number of jets to be determined. Larger numbers of jets are likely in more extreme parameter regimes and with larger density contrasts and therefore will require higher resolutions and longer run times than used in these simulations.

4. Discussion

Expanding Fig. 5, to include the results from Evonuk (2008) and the estimated values for several planetary cores, appears to support the previously noted trend ($Ro_c \propto \chi_\rho^{3/2}$) in spite of slightly different boundary conditions used in the simulations of Evonuk (2008) (the inclusion of a thin subadiabatic region at the outer edge of the disk) (Fig. 7). Note that the five transitional cases at $\chi_\rho = 56$ were previously recorded in Evonuk (2008) as either dipolar or two-jet structured based on their time-averaged behavior, here they are classified as transitional due to their time-dependence. Additionally the two-jet and three-jet cases of Evonuk (2008) are both plotted as differential flows. Table 1 shows the estimated values of the convective Rossby number and density contrast for planetary cores plotted in Fig. 7 (and Fig. 8).

Estimates for the convective Rossby number are based on the buoyancy flux-based Rayleigh numbers from Olson and Christensen (2006), estimates for the density contrasts in the giant planets are based on taking an upper limit of the convective zone at 10^9 Pa (entirely arbitrary, taking a smaller upper bound in pressure will result in a larger density contrasts, i.e. an upper boundary of 10^8 Pa for Jupiter would result in a density contrast of over 200), while estimates for the density contrasts for the rocky/icy planets are obtained from multiple sources (Gudkova and Zharkov, 2002; Rivoldini et al., 2009; Sohl et al., 2001; Zharkov and Gudkova, 2000).

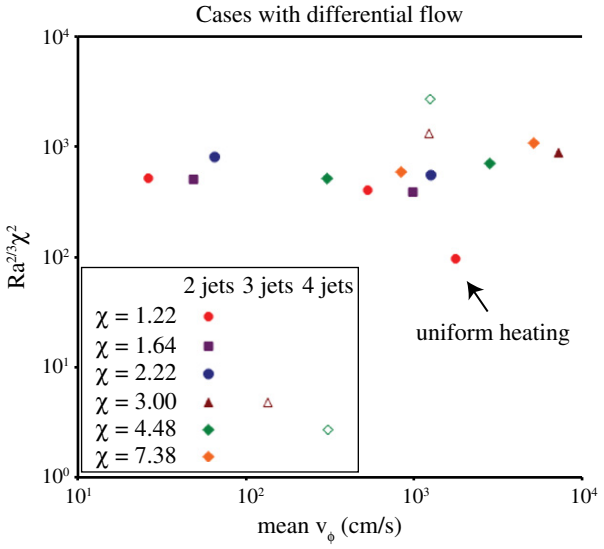

Fig. 6. Log–log plot of the mean tangential velocity (zonal velocity) versus $Ra^{2/3}\chi^2$ for the differential cases. The density contrast, χ, of each case is indicated in the key. Obvious outliers of this trend include the $\chi = 1.22$ case with uniform heating and cases with more than two jets.

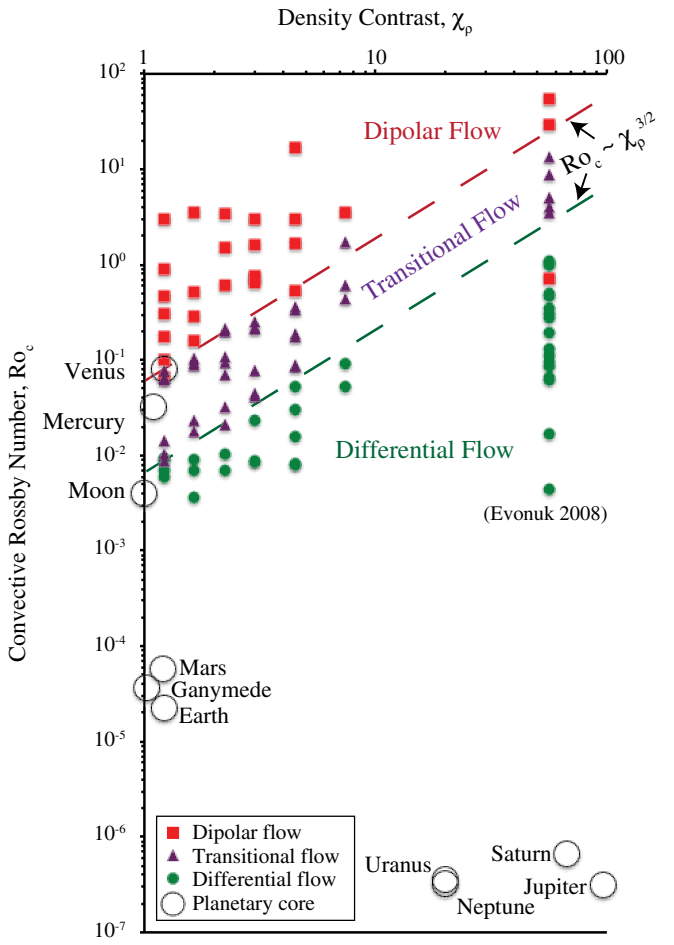

Fig. 7. Log–log plot of density contrast versus convective Rossby number expanded to include all simulations plus the results of Evonuk (2008) and the values estimated for the planets in Table 1. Symbols are as in Fig. 3, with the planets shown in large open circles and labeled appropriately. Again dashed lines show the transition between regimes with the relationship $Ro_c \propto \chi_\rho^{3/2}$. Most planets are still far from the simulated regime, however Mercury appears in the transitional flow regime while Venus lies at the interface of the transitional and dipolar regimes.

These estimates of course fail to account for any stably-stratified regimes that may exist in the convective regions of these planets, for example as hypothesized for Venus.

Notice also that there is a large gap between the largest density contrast modeled in this paper, 7.39, and that of Evonuk (2008), 56. Unfortunately, 7.39 was the largest density contrast that could be modeled at the resolution 400×400 and it was too computationally expensive to run additional cases at higher resolution (simulations of Evonuk (2008) were run with resolutions up to 1600×1600).

Table 1
Parameter regimes of various planetary cores.

Planet	Ro_c (Convective Rossby number)	χ_ρ (Density contrast)	C value
Venus	8.08×10^{-2}	1.22	5.99×10^{-2}
Mercury	3.21×10^{-2}	1.1	2.79×10^{-2}
Earth	2.21×10^{-5}	1.22	1.64×10^{-5}
Mars	5.71×10^{-5}	1.2	4.34×10^{-5}
Jupiter	3.17×10^{-7}	>96	$<3.37 \times 10^{-10}$
Saturn	6.58×10^{-7}	>67	$<1.20 \times 10^{-9}$
Uranus	3.54×10^{-7}	>20	$<3.96 \times 10^{-9}$
Neptune	3.22×10^{-7}	>20	$<3.60 \times 10^{-9}$
Moon	4.04×10^{-3}	~1	4.04×10^{-3}
Ganymede	3.61×10^{-5}	1.03	3.45×10^{-5}

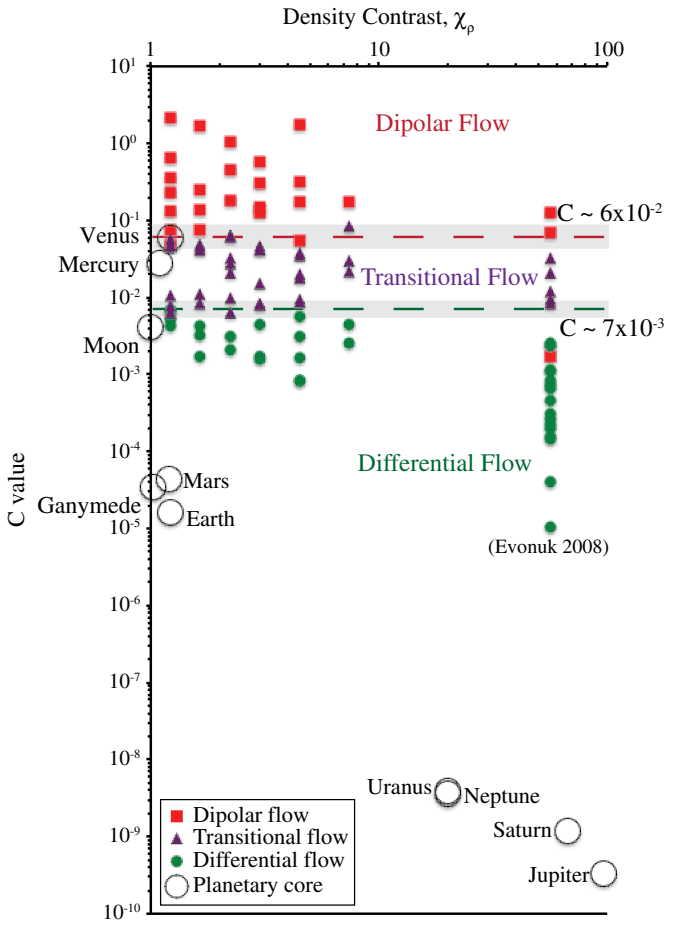

Fig. 8. Log–log plot of the density contrast versus the C value ($Ro_c\chi_\rho^{-3/2}$) for all the simulations and the planets. Symbols are defined as in Fig. 3. Dashed lines are shown at $C \sim 6\times10^{-2}$ and $C \sim 7\times10^{-3}$, the approximate transitions between the three regimes. Gray shaded areas bracketing these lines show regions of overlap in the flow behavior.

A constant can be calculated to mark the transition between the three flow regimes, $C = Ro_c/\chi_\rho^{1.5}$ (where again the exponents are a best fit to the simulation data); the density contrast versus the value of C is plotted for the simulations and the planetary cores (Fig. 8). The estimated C values for the planetary cores are also included in Table 1. Values of C greater than $\sim 6\times10^{-2}$ correspond to fluid behavior in the dipolar flow regime, while values of C less than $\sim 7\times10^{-3}$ correspond to fluid behavior in the differential flow regime. These are approximate values and there can be some overlap between the three regions. This can be seen best for $\chi_\rho = 1.22$, for which the largest number of cases was run, overlap in flow behavior is seen on both sides of the transitional flow regime. This overlap is highlighted by the gray shaded areas in Fig. 8 showing that the changeover from one type of flow behavior to another is more gradual than distinct.

Jupiter and the other giant planets, as predicted by Evonuk (2008), lie firmly in the differential flow regime. The surprising result however, is that of the Earth's outer core, which also appears to lie in the region of differential flow, a result that was unexpected for such a small change in the density. These initial results point towards the Earth's outer core being in a parameter regime where LVDS vorticity generation can play an important role in generating differential rotation. Ganymede and Mars also lie in the differential flow regime, while Mercury lies in the transitional flow regime. Venus is located on the boundary between the transitional and dipolar regions indicating LVDS vorticity formation is likely to be negligible there. The Moon, if it has a density contrast of one, strictly speaking should not feel any effects from LVDS vorticity generation, however if the density changes at all with radius, the Moon would fall near the boundary of the differential and transitional regimes.

It is important to note that this scaling law, while convenient, represents a jump through several orders of magnitude for most planetary bodies (see Figs. 4, 7 and 8). While Venus, Mercury and the Moon lie approximately in the simulated convective Rossby regime (though not in the simulated Ek and Ra regime), simulations are far from the regimes of the other planets. These simulations however help to develop a physical intuition for the nature of the fluid flow in rotating systems, while recognizing that more extreme cases (in turbulence, rotation rate, and density contrast) may experience somewhat different dynamic rules and possibly regimes. As Figs. 4, 7 and 8 (and Table 1) demonstrate, the actual parameter regimes of these bodies still lie beyond the reach of even 2D simulations, let alone 3D simulations. Therefore results should be recognized to be extrapolated out to these highly turbulent bodies. While there may be additional flow regimes possible between the simulated results and the parameter regime of the bulk of the planets, there is no reason to assume the role of LVDS vorticity generation will decrease again as C continues to decrease, therefore it is safe to assume that vorticity generation via movement through a density stratification will continue to increase in importance as the C value decreases.

5. Conclusions

A power law relationship exists between the convective Rossby number and the density contrast such that a value C can be used to determine the behavior of a rotating convective fluid in the two-dimensional equatorial plane. As the value of C decreases, the local generation of vorticity as fluid parcels move with respect to the background density stratification in the rotating disk (LVDS), becomes increasingly dominant in determining the fluid flow pattern. High values of C correspond to dipolar flow patterns, while low values of C correspond to differential flow patterns. This correlation holds for simulations with central heating or uniform heating, and for simulations with varying Prandtl number.

Keeping in mind that this is an extrapolation, a body's value of C can be calculated based on estimates of its parameters to determine if the density stratification needs to be included in simulations. Giant planets are seen to lie in the region of differential flow (therefore including the density stratification is likely very important), while surprisingly the Earth's outer core also appears to lie in the differential flow region. This indicates that LVDS vorticity generation could be playing a role in forming differential rotation in the Earth's outer core and therefore in the production and maintenance of the geomagnetic field. Likewise, LVDS may be important in Ganymede and could play some role in Mercury, but is likely not to play an important role in Venus.

It is also important to note that these simulations were done without a non-convecting inner core. While this may be the case in the early histories of some planets, and currently for others (i.e. some extrasolar planets), most planets currently simulated do possess a core of some size. While a core would hamper the formation of a dipolar flow structure, the diagnostic used here, it is likely not to effect when LVDS, a local form of vorticity generation, becomes important, therefore the C value should still provide a good estimate for this transition in planets with cores.

LVDS vorticity generation is not the only source of vorticity in a rotating body, Busse rolls (Busse, 1976) are capable of generating vorticity via vortex stretching in constant density or in density-stratified fluids. Using the results here as guidelines, simulations are being conducted to compare the strength of the two mechanisms in three dimensions to determine how relatively important vorticity generation via the density stratification, LVDS, is relative to vortex stretching. These comparisons will naturally be restricted

to less turbulent flows which may well exaggerate the importance of vortex stretching in highly turbulent bodies, nevertheless they will provide a first step towards quantifying the relative importance of these two effects.

Acknowledgments

We would like to thank F. Busse for helpful discussions on the topic, as well as three anonymous reviewers for their constructive comments. Funding for this research was provided by a Deutsche Forschungsgemeinschaft (DFG) grant EV 166/1-1. Computations were run on the cluster at the Universität Bayreuth Rechenzentrum and on the cluster of H. Samuel at the Bayerisches Geoinstitut. H Samuel also acknowledges the funds from the Stifterverband fŸr die Deutsche Wissenchaft.

References

Anufriev, A., Cupal, I., 2001. Characteristic amplitudes in the solution of the anelastic geodynamo model. Phys. Earth Planet. Inter. 124, 167–174.
Anufriev, A., Jones, C., Soward, A., 2005. The Boussinesq and anelastic liquid approximations for convection in the earth's core. Phys. Earth Planet. Inter. 152, 163–190.
Aubert, J., Wicht, J., 2004. Axial vs. equatorial dipolar dynamo models with implications for planetary magnetic fields. Earth Planet. Sci. Lett. 221, 409–419.
Aurnou, J., Olson, P., 2001. Experiments on Rayleigh–Benard convection, magnetoconvection and rotating magnetoconvection in liquid gallium. J. Fluid Mech. 430, 283–307.
Brummell, N.H., Hurlburt, N.E., Toomre, J., 1998. Turbulent compressible convection with rotation. ii. mean flows and differential rotation. Astrophys. J. 493, 955–969.
Busse, F., 1976. A simple model of convection in the Jovian atmosphere. Icarus 20, 255–260.
Christensen, U., 2001. Zonal flow driven by deep convection in major planets. Geophys. Res. Lett. 28, 2553–2556.
Christensen, U., 2002. Zonal flow driven by strongly supercritical convection in rotating spherical shells. J. Fluid Mech. 470, 115–133.
Christensen, U.R., Aubert, J., 2006. Scaling properties of convection driven dynamos in rotating spherical shells and application to planetary magnetic fields. Geophys. J. Int. 166, 97–114. doi:10.1111/j.1365- 246X.2006.03009.x.
Evonuk, M., 2008. The role of density stratification in generating zonal flow structures in a rotating fluid. Astrophys. J. 673, 1154–1159.
Evonuk, M., Glatzmaier, G., 2006. A 2d study of the effects of the size of a solid core on the equatorial flow in giant planets. Icarus 181, 458–464.
Gilman, P., 1977. Non-linear dynamics of boussinesq convection in a deep rotating spherical shell. Geophys. Astrophys. Fluid Dyn. 8, 93–135.
Glatzmaier, G., 2005. Planetary and stellar dynamos: challenges for next generation models. In: Soward, A., Jones, C., Hughes, D., Weiss, N. (Eds.), Fluid Dynamics and Dynamos in Astrophysics and Geophysics. CRC Press, pp. 331–357.
Glatzmaier, G.A., Evonuk, M., 2006. Planetary rotation and fluid motion in giant planets: Three numerical modeling approaches. In: Kupka, F., Roxburgh, I., Chan, K. (Eds.), Proceedings IAU Symposium, 239. Cambridge University Press.
Glatzmaier, G., Roberts, P., 1996. Rotation and magnetism of earth's inner core. Science 274, 1887–1891.
Glatzmaier, G., Evonuk, M., Rogers, T., 2009. Differential rotation in giant planets maintained by density-stratified turbulent convection. Geophys. Astrophys. Fluid Dyn. 103, 31–51.
Gudkova, T., Zharkov, V., 2002. The exploration of the lunar interior using torsional oscillations. Planet. Space Sci. 50, 1037–1048.
Guervilly, C., Cardin, P., Schaeffer, N., 2011. A dynamo driven by zonal jets at the upper surface: applications to giant planets. Icarus.
Heimpel, M., Aurnou, J., Al-Shamali, F., Gomez Perez, N., 2005. A numerical study of dynamo action as a function of spherical shell geometry. Earth Planet. Sci. Lett. 236, 542–557.
Jones, C., Kuzanyan, K., 2009. Compressible convection in the deep atmospheres of giant planets. Icarus 204, 227–238.
Jones, C., Rotvig, J., Abdulrahman, A., 2003. Multiple jets and zonal flow on Jupiter. Geophys. Res. Lett. 30, 4. doi:10.1029/2003GL016980.
Julien, K., Legg, S., McWilliams, J., Werne, J., 2001. Rapidly rotating turbulent Rayleigh–Benard convection. J. Fluid Mech. 322, 243–273.
Kaspi, Y., Flierl, G., Showman, A., 2009. The deep wind structure of the giant planets: results from an anelastic general circulation model. Icarus 202, 525–542.
King, E., Stellmach, S., Noir, J., Hansen, U., Aurnou, J., 2009. Boundary layer control of rotating convection systems. Nature 457, 301–304.
Olson, P., Christensen, U., 2006. Dipole moment scaling for convection-driven planetary dynamos. Earth Planet. Sci. Lett. 250, 561–571.
Olson, P., Coe, R., Driscoll, P., Glatzmaier, G., Roberts, P., 2010. Geodynamo reversal frequency and heterogeneous core-mantle boundary heat flow. Phys. Earth Planet. Inter. 180, 66–79. doi:10.1016/j.pepi.2010.02.010.
Rivoldini, A., Van Hoolst, T., Verhoeven, O., 2009. The interior structure of mercury and its core sulfur content. Icarus 201, 12–30.
Rotvig, J., Jones, C., 2006. Multiple jets and bursting in the rapidly rotating convecting two-dimensional annulus model with nearly plane-parallel boundaries. J. Fluid Mech. 567, 117–140.
Sarson, G., Jones, C., 1999. A convection driven geodynamo reversal model. Phys. Earth Planet. Inter. 111, 3–20.
Schaeffer, N., Cardin, P., 2006. Quasi-geostrophic kinematic dynamos at low magnetic Prandtl number. Earth Planet. Sci. Lett. 245, 595–604.
Schmitz, S., Tilgner, A., 2009. Heat transport in rotating convection without Ekman layers. Phys. Rev. E 80, 015305.
Sohl, F., Spohn, T., Breuer, D., Nagel, K., 2001. Implications from Galileo observations on the interior structure and chemistry of the Galilean satellites. Icarus 157, 104–119. doi:10.1006/icar.2002.6828.
Sreenivasan, B., Jones, C., 2006. Azimuthal winds, convection and dynamo action in the polar region of the planetary cores. Geophys. Astrophys. Fluid Dyn. 100, 319–339.
Stanley, S., Glatzmaier, G., 2010. Dynamo models for planets other than earth. Space Sci. Rev. 152, 617–649.
Stanley, S., Bloxham, J., Hutchison, W.E., Zuber, M., 2005. Thin shell dynamo models consistent with Mercury's weak surface magnetic field. Earth Planet. Sci. Lett. 234, 27–38.
Stellmach, S., Hansen, U., 2010. Turbulent rotating Rayleigh–Bénard convection. In: Münster, G., Wolf, D., Kremer, M. (Eds.), NIC Symposium, vol. 3, pp. 305–312.
Vočadlo, L., Alfe, D., Gillan, M., Wood, I., Brodholt, J., Price, G., 2003. Possible thermal and chemical stabilisation of body-centred-cubic iron in the earth's core. Nature 424, 536–539.
Zharkov, V., Gudkova, T., 2000. Interior structure models, Fe/Si ratio and parameters of figure for Mars. Phys. Earth Planet. Inter. 117, 407–420.